Materials Today: Proceedings xxx (xxxx) xxx

Contents lists available at ScienceDirect

Materials Today: Proceedings

journal homepage: www.elsevier.com/locate/matpr

Fabrication of photoanodes using sol-gel synthesized Ag-doped TiO_2 for enhanced DSSC efficiency

K. Balachandran [a,*], T. Kalaivani [b], D. Thangaraju [c], S. Mageswari [a], M.S. Viswak Senan [a], A. Preethi [a]

[a] Department of Chemistry, Vivekanandha College of Engineering for Women, Namakkal, Tamil Nadu, India
[b] Department of Chemistry, VSB Engineering College, Karur, Tamil Nadu, India
[c] Nano-Crystal Design & Application Lab (NCDAL), Department of Physics, PSG Institute of Technology and Applied Research, Coimbatore, Tamil Nadu, India

ARTICLE INFO

Article history:
Received 6 May 2020
Received in revised form 16 May 2020
Accepted 19 May 2020
Available online xxxx

Keywords:
Nanocomposites
Eosin-Y
Ruthenium complex
Blue shift
Quantum confinement effect
Power conversion efficiency

ABSTRACT

A simple, less time consuming, the cost-ineffective sol-gel method was used to synthesis TiO_2 nanoparticles (TiO_2) and Ag-doped TiO_2 nanocomposites (Ag-TiO_2) by using titanium tetra isopropoxide as TiO_2 and silver nitrate as Ag precursors, respectively. The XRD results show that the doping of Ag reduces the grain size from 19 nm to 12 nm. From the UV–Visible, the blue shift in absorbance was confirmed, and there is an increase in bandgap from 3.3 eV to 3.5 eV while increasing the Ag doping in TiO_2. SEM analysis of pure TiO_2 and 10% Ag doped TiO_2 self assembled grains composed of small TiO_2 particles and EDX confirms the presence of Ag in the TiO_2 system. The TEM analysis of 10% Ag doped TiO_2 sample shows that all the particles are in the nanometer range. The power conversion efficiency (PCE) was found to be 4.09%, and 5.6% for N_3 (*cis*-di(thiocyanato)bis(2,2′-bipyridyl 4,4′-di carboxylate ruthenium (II)) containing acetonitrile dye) sensitized TiO_2 and Ag-TiO_2 nanocomposites respectively.
© 2020 Elsevier Ltd. All rights reserved.
Selection and peer-review under responsibility of the scientific committee of the International Conference on Newer Trends and Innovation in Mechanical Engineering: Materials Science.

1. Introduction

Solar energy is considered as one of the best energy resources among all renewable energy resources because it is readily available in all days, and it has been utilized for most of the applications. In recent years nanomaterials and their applications are getting a more and more critical role in solar energy conversion, air purification, wastewater treatment [1], photocatalysis [2,3], electrochemical devices [4] and sensor devices [5,6].

Dye-sensitized solar cells (DSSCs) is a unique device for the conversion of visible light into electricity based on broad bandgap semiconductor sensitization and belongs to a group of thin-film cells [7–10]. DSSCs are a remarkable alternative to silicon-based solar cells because of their relatively high energy conversion efficiency and low cost. A DSSC is based on a semiconductor formed between a photosensitized anode and an electrolyte, a photochemical system. DSSC differs from conventional semiconductor devices by way of separating the function of light absorption from charge carrier transport. Dye sensitizer absorbs the incident sunlight and exploits the light energy to induce electron transport. In DSSC, electron transport takes place from dye to semiconductor [11].

Recently, nanosized TiO_2 powders have been used as a working electrode for dye-sensitized solar cells due to their higher efficiency than any other metal oxide semiconductor. However, as reported, the best TiO_2 solar efficiency could hardly reach 11.5% [12]. Additionally, TiO_2 has proven to be the most suitable for widespread solar energy conversion and environmental applications due to its biological, chemical inertness, strong oxidizing power, cost-effectiveness, long term stability against photo corrosion and chemical corrosion [13].

Titania compounds doped with silver have been synthesized for antibacterial and photoelectrochemical applications [14,15]. Indeed, TiO_2 doped with silver nanoparticles have shown improved photocatalytic activity compared with its undoped counterpart [16,17]. It was proposed that Ag doping of TiO_2 improves charge transfer and charge pair separation efficiency [18].

There are many approaches to synthesize TiO_2 and modified TiO_2 [19], including hydrothermal [20], electrochemical [21], microwave [22], sonochemical [23] and sol–gel methods [24]. Among these methods, the sol–gel method offers simple methodology, high control of the surface area, average crystallite size, phase structure, and morphology [25,26].

* Corresponding author.
E-mail address: balanano06@gmail.com (K. Balachandran).

https://doi.org/10.1016/j.matpr.2020.05.485
2214-7853/© 2020 Elsevier Ltd. All rights reserved.
Selection and peer-review under responsibility of the scientific committee of the International Conference on Newer Trends and Innovation in Mechanical Engineering: Materials Science.

Please cite this article as: K. Balachandran, T. Kalaivani, D. Thangaraju et al., Fabrication of photoanodes using sol-gel synthesized Ag-doped TiO_2 for enhanced DSSC efficiency, Materials Today: Proceedings, https://doi.org/10.1016/j.matpr.2020.05.485

In DSSC, the counter electrode is a significant part of improving electron transportation. It should be chemically inert, stable, non-corrosive, and exhibit excellent catalytic activity for the reduction of tri-iodide ion. As a result, many types of carbonaceous materials such as carbon nanotubes [27] carbon black [28] and graphite [29] were used as a counter electrode.

In the present work, we synthesized TiO_2 and Ag-TiO_2 nanocomposites by the Sol-gel method, and it was characterized by XRD, UV–Visible, SEM, and TEM analysis. The photovoltaic performances of N_3 dye-sensitized TiO_2 and Ag-TiO_2 photoanodes were studied by using carbon-coated FTO as a counter cathode. The study also reveals that the effect of doping Ag in TiO_2 particles.

2. Materials and methods

2.1. Synthesis of TiO_2 nanoparticles

Titanium tetra isopropoxide (TTIP) was used as a precursor, Hydrochloric acid (HCl) as a peptizing agent and ethanol were used as the solvent medium. HCl was mixed with ethanol and was stirred for a few minutes. To this mixture, TTIP was added in the ratio of 1:4:2, and the stirring were continued for 1 h at room temperature. Then 100 mL of distilled water was added, the temperature was raised to 50 °C and stirred for 3 h until the solution changed into a colorless gel. The high viscous gel was dried at room temperature to a fine powder. The resulting powder was heated at 120 °C for 1 h in a hot air oven. Finally, the colorless powder was calcined at 400 °C for 2 hr.

2.2. Synthesis of Ag-doped TiO_2 nanoparticles

The TiO_2 solution was prepared by the above-said method. To this solution, $AgNO_3$ solutions at various concentrations (2.5–10%) were added to form Ag-TiO_2 composites.

The concentration of silver nitrate solution was varied from 2.5% to 10% at steps of 2.5%. The total concentration of the solution was maintained at 0.1 mol/liter. Silver nitrate solution was added to the above solution with (Ag/Ti) nominal volume proportions 2.5, 5, 7.5, and 10%, and stirring was continued for 3 hr to form Ag-TiO_2 nanocomposites. The fine precipitate washed with deionized water and dried at 120 °C for 1 hr. Then the powder was calcined for 2 h at 400 °C.

2.3. Characterization of synthesized TiO_2 nanoparticles and Ag-TiO_2 nanocomposites

The optical properties of TiO_2 nanoparticles and Ag-TiO_2 nanocomposites were characterized by UV–Visible spectroscopy (Carry 5000 UV–Vis-NIR spectrophotometer, Varian, USA). The crystalline structure of synthesized TiO_2 nanoparticles and Ag-TiO_2 nanocomposites were analyzed using D8 Advance X-ray diffraction meter (Bruker AXS, Germany) at room temperature, operating at 30 kV and 30 mA, using Cu Ka radiation (k = 0.15406 nm) and crystal size was calculated by Scherrer's formula. Surface morphology of synthesized TiO_2 nanoparticles and Ag-TiO_2 nanocomposites were characterized using a scanning electron microscope (SEM) (Model JSM 6390LV, JOEL, USA). The

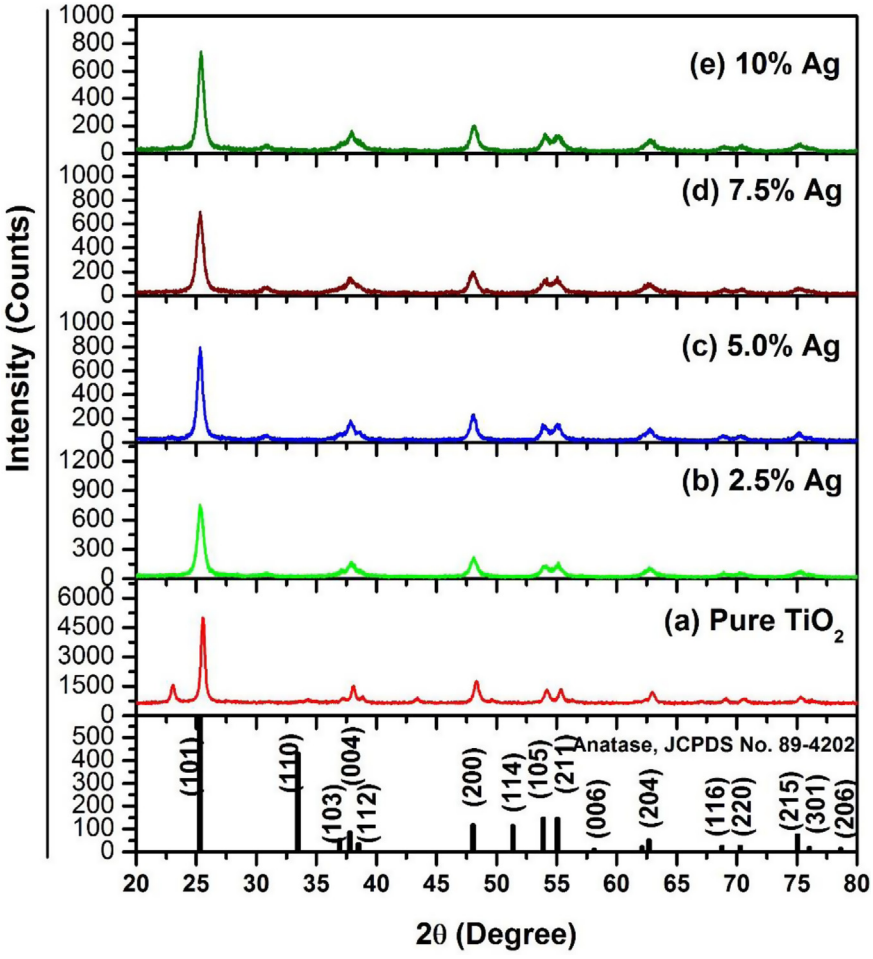


Fig. 1. XRD patterns of TiO_2 and Ag-TiO_2 nanocomposites.

Please cite this article as: K. Balachandran, T. Kalaivani, D. Thangaraju et al., Fabrication of photoanodes using sol-gel synthesized Ag-doped TiO_2 for enhanced DSSC efficiency, Materials Today: Proceedings, https://doi.org/10.1016/j.matpr.2020.05.485

Table 1
The structural properties of TiO_2 and Ag-TiO_2 nanocomposites.

	Pos. [°2Th.]	d-spacing [Å]	FWHM [°2Th.]	H	K	L	Lattice constant (Å)		Grain size (nm)	Micro strain (ε) 10^4 $lin^{-2}m^{-4}$	Dislocation density $10^{15}lin/m^2$
							a	**c**			
TiO_2	25.557	3.486	0.427	1	0	1	3.798	9.531	19.90	18.10	2.52
	38.012	1.890	0.345	1	1	2			25.40	14.20	1.54
	48.020	1.899	0.167	2	0	0			54.50	6.60	33.60
	55.351	1.660	0.475	2	1	1			19.70	18.30	2.56
	62.963	1.476	0.546	2	0	4			17.80	20.30	3.14
	70.640	1.333	0.185	2	2	0			55.10	6.50	32.90
	75.330	1.262	0.461	2	1	5			22.70	15.90	1.93
2.5% Ag- TiO_2	35.363	3.506	0.639	1	0	1	3.813	9.383	13.30	27.20	5.64
	48.090	1.891	0.760	2	0	0			10.80	33.40	8.55
	54.050	1.695	0.840	2	1	1			9.30	38.80	0.11
	62.550	1.477	1.000	2	0	4			9.70	37.20	0.10
	69.820	1.346	20,280	2	2	0			4.40	81.50	0.50
	75.170	1.263	0.980	2	1	5			10.60	33.80	8.76
5% Ag- TiO_2	25.310	3.516	0.554	1	0	1	3.836	9.338	15.30	23.50	4.24
	48.090	1.891	0.606	2	0	0			14.90	24.10	4.45
	53.980	1.697	0.740	2	1	1			12.50	28.70	6.31
	62.800	1.479	0.930	2	0	4			10.40	34.60	9.15
	69.060	1.359	2.150	2	2	0			4.70	77.20	0.45
	75.030	1.265	0.790	2	1	5			13.20	27.30	5.70
7.5% Ag- TiO_2	25.304	3.517	0.683	1	0	1	3.806	9.409	12.40	29.10	6.45
	48.000	1.894	0.780	2	0	0			11.60	31.10	7.37
	54.510	1.682	1.820	2	1	1			5.10	70.50	0.38
	65.780	1.479	1.120	2	0	4			8.70	41.70	0.13
	69.850	1.345	2.210	2	2	0			4.60	79.10	0.47
	75.190	1.263	1.320	2	1	5			7.90	45.60	0.15
10% Ag- TiO_2	25.373	3.507	0.608	1	0	1	3.811	9.411	13.90	25.80	5.11
	48.070	1.891	0.685	2	0	0			13.20	27.20	5.68
	54.100	1.694	0.700	2	1	1			13.30	27.20	5.64
	62.840	1.478	1.060	2	0	4			9.20	39.40	0.11
	69.840	1.346	2.270	2	2	0			4.50	81.20	0.50
	75.050	1.265	1.320	2	1	5			7.90	45.60	0.15

nanoparticles and composites were viewed through a transmission electron microscope (TEM) (JEOL-TEM 2100) at high magnification, and the exact particle size was predicated.

2.4. Fabrication of DSSC

2.4.1. Preparation of TiO_2 and Ag-TiO_2 electrode and treatment with dye

The thin nanostructured photo-anode film was fabricated using synthesized TiO_2 and Ag-TiO_2 nanocomposites by employing the doctor blade technique. TiO_2 and Ag-TiO_2 nanomaterials were ground by a mortar and pestle with the addition of an appropriate amount of distilled water and methanol. After making a viscous paste, it was further diluted with distilled water, and then a few drops of triton X-100 was added for better adhesion of the paste on conducting substrate. The paste was spread on the conducting substrate with a glass rod using adhesive tape as spacers. After drying in air, the film was sintered for 30 min at 400 °C in a muffle furnace. After sintering, the TiO_2 and Ag-TiO_2 film were sensitized in 0.5 mM of N_3 dye-containing acetonitrile dye solution for 18 h. The dye-sensitized electrodes were rinsed with acetonitrile to remove excess unanchored dye molecules on the surface.

2.4.2. Preparation of counter electrode

The preparation of counter electrodes followed the method described in [28]. EG (130 mg) was respectively mixed with different weight 5B pencil-lead according to the weight ratios. To each 130 mg mixture, 0.6 mL TiO_2 colloid, 1.2 mL water, 0.6 mL 10% Triton X-100 aqueous solution, and 1 mL ethanol were added. After milling for an hour, the carbon counter electrode pastes were obtained. It was then coated on the FTO conductive glass using the doctor blade technique. After dried for 30 min at room temperature, the substrate was heated at 450 °C for an hour. So the carbon counter electrode was prepared.

2.4.3. Electrolyte preparation

The electrolyte solution was composed of 0.5 M LiI/0.05 M I/0.5 M TBP (Tetra butyl pyridine), it was prepared by 0.63 g of iodine (Mol. Wt. = 126.9), 6.7 g of lithium iodide (LiI) (Mol.Wt. = 133.8) and 9.5 g of TBP (Mol. Wt. = 191.3) dissolved in 100 mL of acetonitrile solution.

2.4.4. Assembly of TiO_2 based DSSC

DSSC was fabricated using standard two-electrode configurations, comprising dye-sensitized TiO_2/FTO (with an active surface area of 0.25 cm^2) as a photoanode, carbon-coated FTO as a counter electrode. For two-electrode measurement, the liquid electrolyte I^-/I_3^- was injected between photoanode and counter cathode, pressing firmLy. A thin layer of parafilm was used as a spacer to avoid short-circuiting between two electrodes. A binder clip was fixed externally to maintain the mechanical grip of the cell without any further sealing, which finalized the assembly of the DSSC. The V- I characteristics of current was measured by Keithley electrometer under the light radiation source of 1000 mW/cm^2. The following cell configurations were used to record I–V plots: FTO/TiO_2/N3-Dye/I^-/I_3^-/C/FTO and FTO/Ag-TiO_2/N3-Dye/I^-/I_3^-/C/FTO.

3. Results and discussion

3.1. X-ray diffraction of TiO_2 nanoparticles and Ag-TiO_2 nanocomposites

The x-ray diffraction patterns of the undoped TiO_2 and Ag -TiO_2 nanocomposites are shown in Fig. 1. The nanocrystalline anatase structure was confirmed by (1 0 1), (1 1 0), (1 0 3), (0 0 4), (1 1 2), (2 2 0), (1 1 4), (1 0 5), (2 1 1), (2 0 4), (1 1 6), (2 2 0), (3 0 1) and (2 0 6) diffraction peaks [28]. The XRD patterns of anatase have main diffractions at 2θ = 25.3° corresponding to the 101 planes

Please cite this article as: K. Balachandran, T. Kalaivani, D. Thangaraju et al., Fabrication of photoanodes using sol-gel synthesized Ag-doped TiO_2 for enhanced DSSC efficiency, Materials Today: Proceedings, https://doi.org/10.1016/j.matpr.2020.05.485

when compared to JCPDS card No.21–1272, respectively. Therefore, rutile and brookite phases have not been detected [30]. The x-ray diffraction patterns of the Ag -TiO_2 nanocomposites (Fig. 1a to e) coincides with the pure TiO_2 and show no diffraction due to the silver species, thus suggesting that silver particles are well dispersed on the TiO_2 surface. Doping with silver does not disturb the crystal structure of anatase TiO_2, that the silver dopants are merely placed on the surface of the crystal without being covalently anchored into the crystal lattice. There are no diffraction pattern characteristics of the silver in the XRD patterns. The diffraction patterns of pure TiO_2 and Ag -TiO_2 nanocomposites showed considerable line width, indicating small particles. The crystallite size D was calculated from the full width at half maximum (FWHM) of the (1 0 1) diffraction peak using Scherrer's equation.

$$D = \frac{K\lambda}{\beta\cos\theta} \quad (1)$$

where D is average crystal size, λ the X-ray wavelength (1.54056 Å), β the fullwidth at half maximum (FWHM) of the diffraction peak (radian), K is a coefficient (0.89), and θ is the diffraction angle at the peak maximum. All prepared samples are in the nano-size range, from 9 to 12 nm, further it was found that doping of Ag in TiO_2 reduces the grain size, which is shown in Table 1. The shifted Ag-TiO_2 nanocomposites peaks are shown in Fig. 2. It is observed in Fig. 2 that the intensity of the peaks shifted to the lower angle side with an increase in Ag concentrations. The structural properties of Ag-TiO_2 nanocomposites are listed in Table 1.

3.2. UV–Visible analysis of TiO_2 and Ag-TiO_2 nanocomposites

Fig. 3. shows the UV–Visible spectra of TiO_2 and Ag-TiO_2 nanocomposites. In all the particles, the absorption was measured

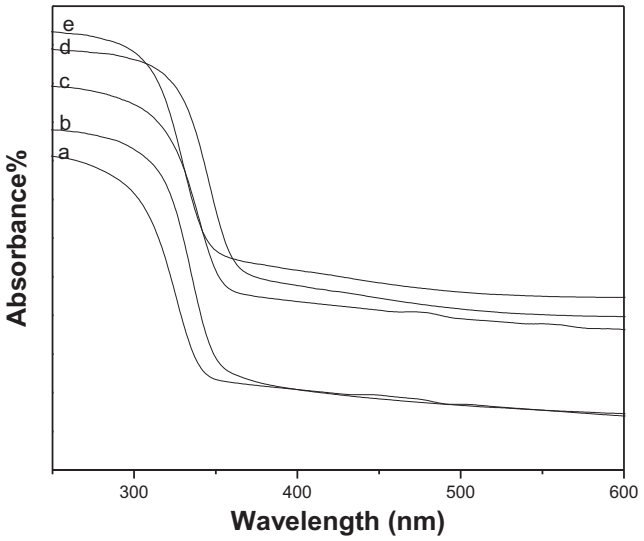


Fig. 3. UV–Visible spectra of TiO_2 (a), 2.3, 5, 7.5 and 10% Ag-TiO_2 (b–e) nanocomposites.

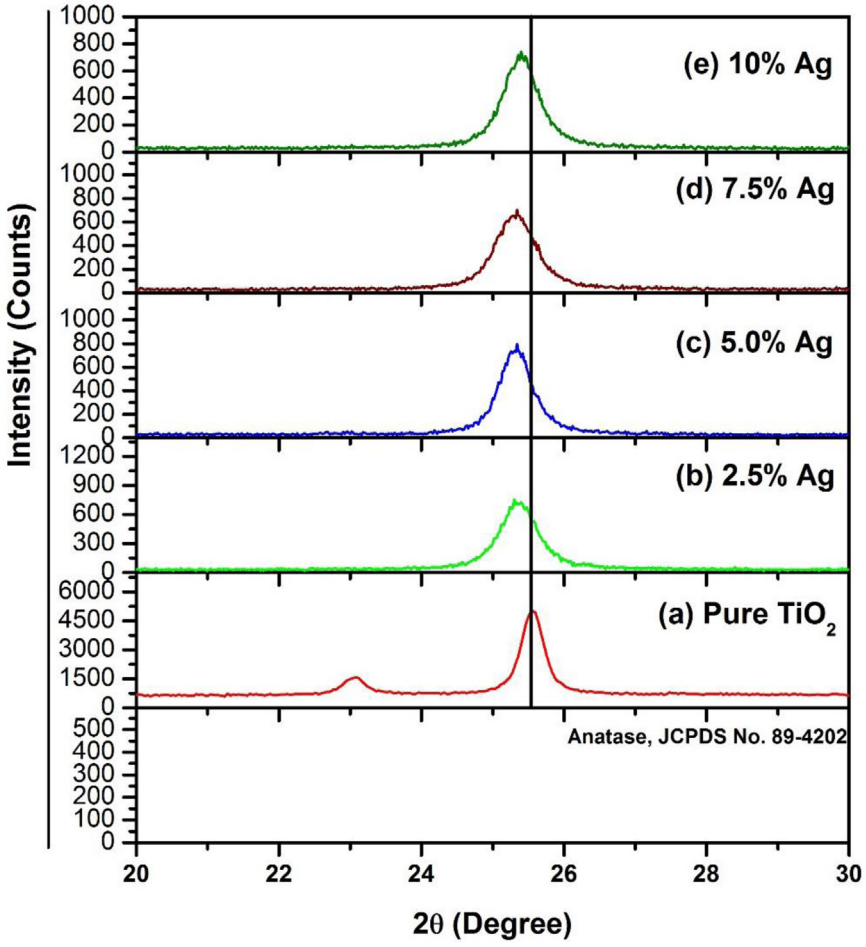


Fig. 2. XRD Peaks shift of Ag-TiO_2 nanocomposites.

Please cite this article as: K. Balachandran, T. Kalaivani, D. Thangaraju et al., Fabrication of photoanodes using sol-gel synthesized Ag-doped TiO_2 for enhanced DSSC efficiency, Materials Today: Proceedings, https://doi.org/10.1016/j.matpr.2020.05.485

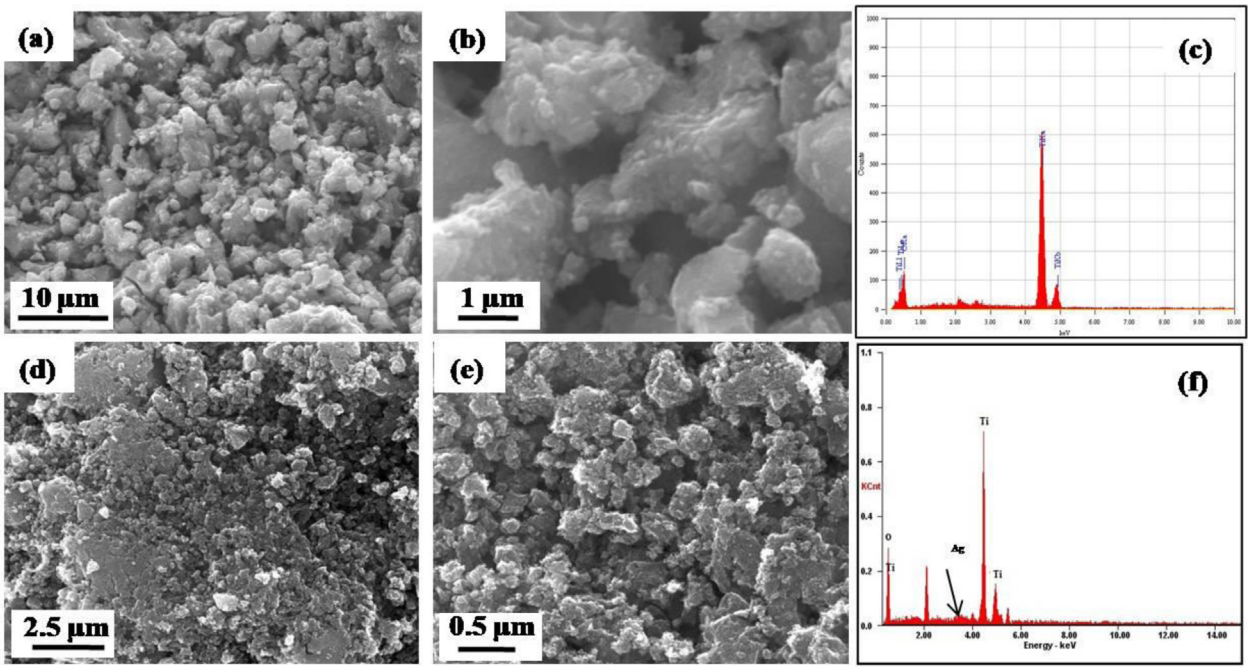


Fig. 4. FESEM and EDS images of TiO_2 (a–c) and 10% Ag-TiO_2 (d–f) nanocomposites.

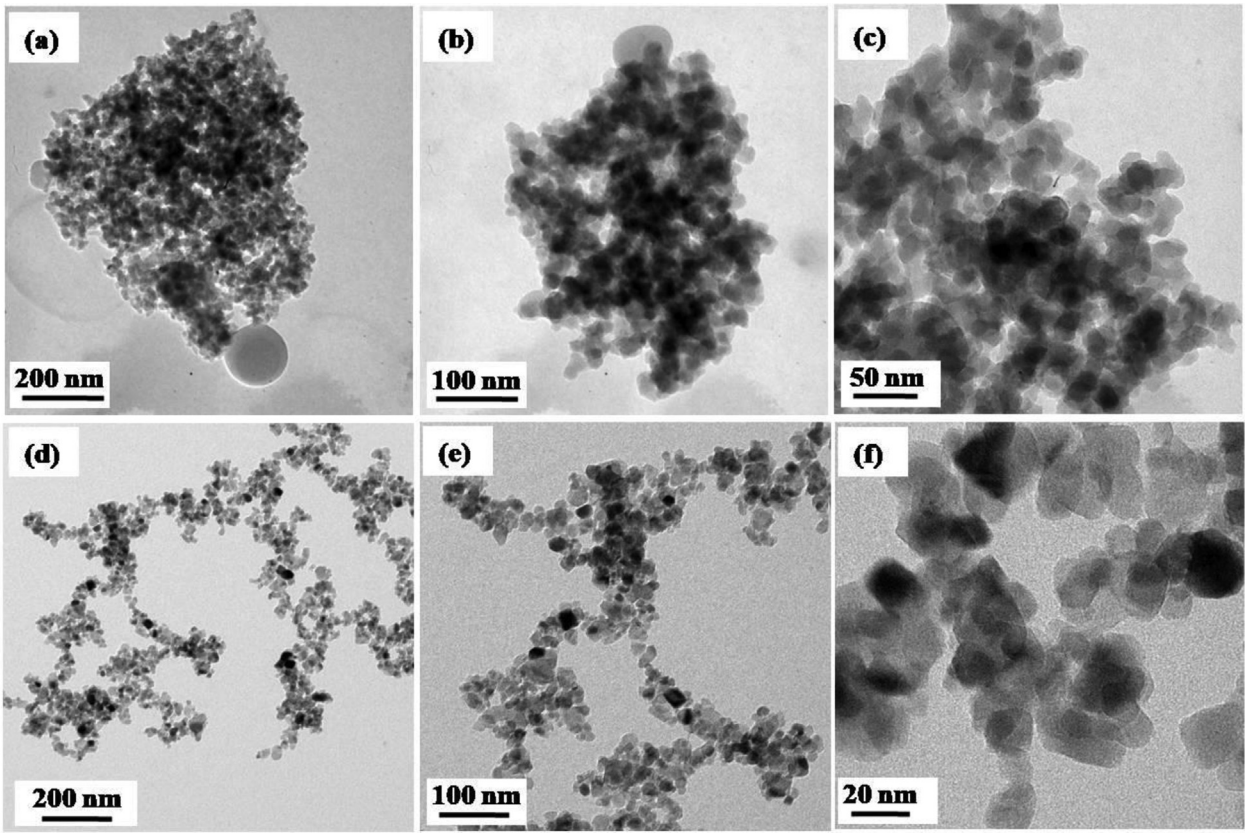


Fig. 5. TEM images of TiO_2 (a–c) and 10% Ag-TiO_2 (d–f) nanocomposites.

in the range between 250 and 600 nm. It is shown that TiO_2 is an oxide semiconductor, and its anatase form has an optical absorbance range around 384 nm, bandgap 3.2 eV. In the current measurement, the onset of the absorption peak of maximum absorbance occurred at 372 nm for TiO_2. Further, it decreased with increasing concentrations of Ag. The absorbance was observed at 369, 360, 350, and 342 nm for 2.5, 5, 7.5, and 10% Ag, respectively. The blue shift in absorbance corresponds to a smaller particle size. The blue shift observed in the absorbance spectra indicated the Quantum confinement effect. The absorption edge shifted to the

Please cite this article as: K. Balachandran, T. Kalaivani, D. Thangaraju et al., Fabrication of photoanodes using sol-gel synthesized Ag-doped TiO_2 for enhanced DSSC efficiency, Materials Today: Proceedings, https://doi.org/10.1016/j.matpr.2020.05.485

lower wavelength region confirmed the formation of nano-sized products [31].

The optical bandgap of the material was calculated by effective mass approximation, and it was found to be 3.3, 3.42, 3.45, 3.48, and 3.5 eV for TiO_2, the various concentration of Ag-doped TiO_2 respectively. Further, it was found to be the crystallite size of Ag-doped TiO_2 particles was smaller than pure TiO_2 because of the quantum confinement effect [32].

3.3. FESEM and TEM analysis of TiO_2 and Ag-TiO_2 nanocomposites

Fig. 4 shows the surface morphology and the different magnification image of TiO_2 and Ag-TiO_2 nanocomposites. Granulation of TiO_2: Ag nanoparticles is smooth, dense, with pinholes uniform like grains. For the estimation of the average grain size of particles, a line was drawn on the FESEM image, and its length was divided by the number of grain boundaries crossing the line. The average particle size was found to be ~ 12 nm. The EDS spectrum of TiO_2: Ag nanoparticles are shown in Fig. 4f. The spectrum depicted in Fig. 3f, the TiO_2: Ag nanoparticles have unlabelled peaks due to the coated C and Au. Besides, the spectrum shows the presence of Ag, Ti, and O elements in the materials as expected.Fig. 5.

The TEM analysis was carried out to confirm the actual size of the particles, their growth pattern, and the distribution of the crystallites. The size and morphology of TiO_2: Ag nanoparticles synthesized by TEM images are shown in Fig. 6. It is also revealed the uniform size and spherical shape distribution of TiO_2: Ag is obtained at a high concentration of 10% of Ag with an average diameter of about 12 nm.

3.4. Photovoltaic performances of Dye-Sensitized solar cells

Once the electrons are injected from the photo-excited dye molecules to the conduction band of TiO_2 nanoparticles, their transport dynamics determine the charge-collection efficiency; One of the major factors that contribute to the high-energy conversion efficiency in DSSC is generally attributed to the ultrafast electron injection from dye to the TiO_2 conduction band and a much slower reverse process. The dynamics of electron injection at the dye-TiO_2 interface has been the subject of considerable recent investigations [33]. The current–voltage (I-V) characteristics of DSSC constructed by using TiO_2 particles and Ag-TiO_2 composites sensitized with eosin-Y and N_3 dye under illumination condition

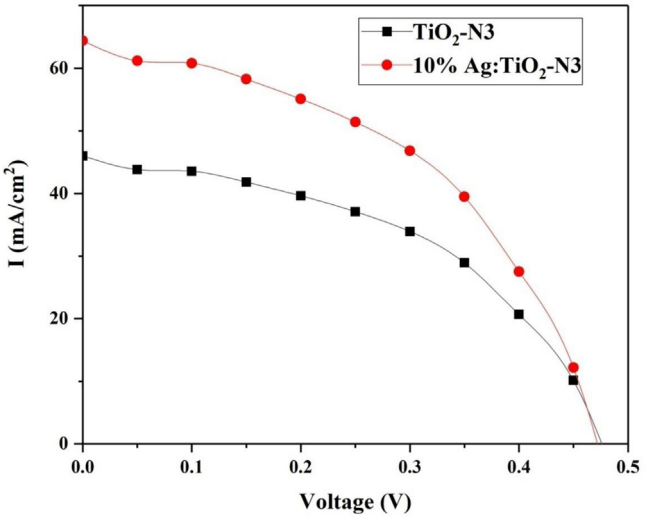


Fig. 6. The I-V characteristics of a) TiO_2-N3, and b) 10% Ag-TiO_2- N3 under light illumination.

(1000 W Cm^{-2}) are shown in Fig. 6. The fill factor and conversion efficiency of the fabricated TiO_2 and Ag-TiO_2 based DSSC is calculated as follows

$$FF = \frac{V_{max} \times J_{max}}{V_{OC} \times J_{SC}} \quad (2)$$

Where,

V_{oc} = open-circuit voltage, J_{sc} = short circuit current,

V_{max} = maximum voltage, J_{max} = maximum current density.

The power conversion efficiency (η) of the fabricated cell is given as follows

$$\eta = \frac{FF \times V_{OC} \times J_{SC}}{P_{in}} \quad (3)$$

Where P_{in} = power input (1000 W/ cm^2)

The Isc, Jsc, Imax, Jmax, Vmax, Voc, FF, and Efficiency of the N3 sensitized TiO_2, and Ag-TiO_2 DDSCs are shown in Table 2.

The porous structure of TiO_2 and Ag-TiO_2 film is an important factor to increase the power conversion efficiency. The porous structure is the supporter of adsorbing dye molecules, and the diffusion path of electrolyte in the DSSCs was generated after the binder Triton X-100 combusted at 400 °C [28]. These pores could increase the surface area of the TiO_2 and Ag-TiO_2 film resulting in a large amount of dye adsorbed on the surface of TiO_2 and Ag-TiO_2 films. Meanwhile, the pores could increase the contact area between dye molecules and the electrolyte contributing to the oxidized dye being reduced immediately by I_3^- in the electrolyte. The DSSC is rather a complicated system, including many processes such as light absorption, charge injection, charge collection, and electrolyte diffusion [34]. The light to the electricity conversion efficiency of the DSSCs is influenced by many factors, such as dyes and dopants. Further, the N_3 dye is a far superior chromophore due to its reduced symmetry relative to the reference $[Ru(bpy)_3]^{2+}$complex; this imparts additional bands in its electronic absorption spectrum improving its light-harvesting properties. These transitions occur further to the red of $[Ru(bpy)_3]^{2+}$ in the visible region, i.e., bathochromically shifted, due to the electron-rich nature of the two monodentate isothiocyanate ligands (NCS) which destabilize the HOMO orbital reducing the bandgap of the molecule.

The role of Ag as an energy barrier in Ag-TiO_2 film is well consistent and supported by the photovoltaic performance data of DSSCs in Fig. 6. and Table 2. Ag-TiO_2 film-based DSSCs show superior photovoltaic performance compared to the bare TiO_2 film counterparts. The open-circuit potential (V_{OC}) is theoretically determined by the difference between the potential of redox electrolytes and the quasi-Fermi level of electrons in TiO_2 in the light, which strongly depends on the density of photo-excited electrons injected from the adsorbed dye, into TiO_2 network. When the TiO_2 based films are calcined at 400 °C, nanoparticles in the TiO_2-based network are subjected to partial sintering that renders them chemically bonded. This process not only increases the charge transport rate due to the enhanced number of interconnections between the particles but also improves the dispersion of photo-excited electrons in the TiO_2 network which could suppress the charge recombination that brings about an increase in the density of photo-excited electrons in the TiO_2-based network and therefore negatively shifts its quasi-Fermi level [35]. The resistance of electrolyte solutions, the charge transfer resistances at the electrolyte/TiO_2 interface, and finally, the resistance of the electrons in the TiO_2 film can be considered. This indicates that the charge transfer resistance was decreased when the TiO_2/Ag-TiO_2/N_3 electrode was used, and this provides evidence that the photocurrent is increased. The charge transfer resistance at the electrolyte/TiO_2 means the charge transfer resistance from excited dye to the TiO_2, and this could be regarded as a relative measure of barrier height of the electron injection from excited dye molecules to

Please cite this article as: K. Balachandran, T. Kalaivani, D. Thangaraju et al., Fabrication of photoanodes using sol-gel synthesized Ag-doped TiO_2 for enhanced DSSC efficiency, Materials Today: Proceedings, https://doi.org/10.1016/j.matpr.2020.05.485

Table 2
PV parameters of DSSCs sensitized with N3 dye.

Sample	I_{sc} (mA/cm^2)	J_{sc} (mA/cm^2)	V_{oc} (V)	I_{max} (mA/cm^2)	J_{max} (mA/cm^2)	V_{max} (V)	FF	η (%)
TiO_2: N3	46.1	184.4	0.471	34.1	136.4	0.3	0.471	4.09
10% Ag-TiO_2: N3	64.5	258.0	0.468	49.6	187.6	0.3	0.466	5.60

the conduction band of the TiO_2. In other words, lower the charge transfer resistance, the larger the electron injection driving force and, consequently, a larger I_{SC} can be obtained.

4. Conclusion

TiO_2 and Ag-TiO_2 nanocomposites were successfully synthesized by the sol–gel method; it was characterized by XRD, SEM, TEM, and UV–Visible analysis. The synthesized nanoparticles and nanocomposites show good photovoltaic performance in N_3 sensitized TiO_2 and Ag-TiO_2. When compared with N_3 sensitized TiO_2, Ag-TiO_2 shows higher efficiency because of low charge transfer resistance and larger electron injection driving force in the Ag-TiO_2 photoanode than TiO_2 photoanode. The study reveals that the doping of Ag in TiO_2 suppresses the grain size, absorbance and increases the bandgap, which increases the PCE in DSSC.

CRediT authorship contribution statement

K. Balachandran: Conceptualization, Methodology, Writing - original draft. **T. Kalaivani:** Data curation. **D. Thangaraju:** Writing - review & editing. **S. Mageswari:** Visualization, Investigation. **M.S. Viswak Senan:** Visualization, Investigation. **A. Preethi:** Visualization, Investigation.

Declaration of Competing Interest

The authors declare that they have no known competing financial interests or personal relationships that could have appeared to influence the work reported in this paper.

References

[1] M. Behpour, M. Mehrzad, S.M. Ghoreishi, S.M.H. Mashkani, J. Mater. Sci.: Mater. Electron. 27 (2016) 4483–4488.
[2] A.S. Nasab, M. Maddahfar, S.M.H. Mashkani, J. Mol. Liq. 216 (2016) 1–5.
[3] V. Santhana, D. Thangaraju, A. Tanaka, W. Inami, S. JayaKumar, S. Matsuda, J. Inorg. Organomet. Polym. (2020), https://doi.org/10.1007/s10904-020-01448-2.
[4] M. Mansournia, S. Rafizadeh, S.M.H. Mashkani, M.H. Motaghedifard, Mater. Sci. Eng., C 65 (2016) 303–312.
[5] R. Kalai Selvan, A. Gedanken, P. Anilkumar, G. Manikandan, C. Karunakaran, J. Cluster Sci. 20 (2009) 291–305.
[6] D. Thangaraju, R. Marnadu, V. Santhana, A. Durairajan, P. Kathirvel, J. Chandrasekaran, S. Jayakumar, M.A. Valente, D.C. Greenidge, CrystEngComm 22 (2020) 525–533.
[7] S. Rühle, M. Shalom, A. Zaban, Chem. Phys. Chem. 11 (2010) 2290–2304.
[8] E. Yamazaki, M. Murayama, N. Nishikawa, N. Hashimoto, M. Shoyama, O. Kurita, J. Sol Energy 81 (2007) 512–516.
[9] Z. Huizhi, L. Wu, Y. Gao, T. Ma, J. Photo Chem. Photo Boil. A Chem 219 (2011) 188–194.
[10] M. Grätzel, J. Photochem. Photobiol., C 4 (2003) 145–153.
[11] Y. Duan, N. Fu, Q. Liu, Y. Fang, X. Zhou, J. Zhang, Y. Lin, J. Phys. Chem. C 116 (2010) 8888–8893.
[12] K.G. Deepa, P. Lekha, S. Sindhu, Sol. Energy 86 (2012) 326–330.
[13] S.S. Mali, C.A. Betty, P.N. Bhosale, P.S. Patil, Electrochim. Acta 59 (2012) 113–120.
[14] K. Ubonchonlakate, L. Sikong, F. Saito, Procedia Eng. 32 (2012) 656–662.
[15] D. Guin, S. Manorama, J. Phys. Chem. C 111 (2007) 13393–13397.
[16] N. Sobana, M. Muruganadham, M. Swaminathan, J. Mol. Catal. A: Chem. 258 (2006) 124–132.
[17] M.K. Seery, R. George, P. Floris, S.C. Pillai, J. Photochem. Photobiol., A 189 (2007) 258–263.
[18] C. He, Y. Yu, X. Hu, A. Larbot, Appl. Surf. Sci. 200 (2002) 2–10.
[19] A.A. Ismail, D.W. Bahnemann, J. Mater. Chem. 21 (2011) 11686.
[20] K. Nagaveni, M.S. Hegde, N. Ravishankar, G.N. Subbanna, G. Madras, Langmuir 20 (2004) 2900–2907.
[21] Z. Miao, D. Xu, J. Ouyang, G. Guo, X. Zhao, Y.X. Tang, Nano Lett. 2 (2004) 717–720.
[22] K. Ding, Z. Miao, Z. Liu, Z. Zhang, B. Han, G. An, S. Miao, Y. Xie, J. Am. Chem. Soc. 129 (2007) 6362–6363.
[23] Y. Zhu, H. Li, Y. Koltypin, Y.R. Hacohen, A. Gedanken, Chem. Commun. 17 (2001) 2616–2617.
[24] M. Zhang, Y. Bando, K. Wada, J. Mater. Sci. Lett. 20 (2001) 167–170.
[25] Z. Jiwei, N. Liangying, Y. Xi, S.N.B. Hodgson, Surf. Coat. Technol. 138 (2001) 135–140.
[26] U.G. Akpan, B.H. Hameed, Appl. Catal. A 375 (2010) 1–11.
[27] G.J. Nam, Y.J. Park, B.S. Kim, J.S. Lee, Scr. Mater. 62 (2010) 148–150.
[28] T.N. Murakami, S. Ito, Q. Wang, M.K. Nazeeruddin, T. Bessho, I. Cesar, P. Liska, R.H. Baker, P. Comte, P. Pechy, M. Grätzel, J. Electrochem. Soc. 153 (2006) 2255–2261.
[29] K. Imoto, K. Takahashi, T. Yamaguchi, T. Komura, J. Nakamura, K. Murata, Sol. Energy Mater. Sol. Cells 79 (2003) 459–469.
[30] S. Kalaiselvan, K. Balachandran, S. Karthikeyan, R. Venckatesh, Silicon 10 (2018) 211–217.
[31] P.K. Khanna, N. Singh, C. Shobhit, Mater. Lett. 61 (2007) 4725–4730.
[32] K. Balachandran RajendranVenckatesh, S. Rajeshwari, P. Rajiv, Spectrochim. Acta Part A Mol. Biomol. Spectrosc. 128 (2014) 468–474.
[33] K.D. Satyen, Sol En Mater Sol Cel 88 (2005) 1–10.
[34] J.T. Jiu, F.M. Wang, M. Sakamoto, J. Takao, M. Adachi, Sol. Energy Mater. Sol. Cells 87 (2005) 77–86.
[35] K. Zhu, T.B. Vinzant, N.R. Neale, A.J. Frank, Nano Lett. 7 (2005) 3739–3746.

Further Reading

[1] E. Olsen, S.E. Lindquist, Sol. Energy Mater. Sol. Cells 63 (2000) 267–273.
[2] Y.S. Wei, Q.Q. Jin, T.Z. Ren, Solid State Electron. 63 (2011) 76–82.

Please cite this article as: K. Balachandran, T. Kalaivani, D. Thangaraju et al., Fabrication of photoanodes using sol-gel synthesized Ag-doped TiO_2 for enhanced DSSC efficiency, Materials Today: Proceedings, https://doi.org/10.1016/j.matpr.2020.05.485